molecules

MDPI

Article

Preparation of Sulfonated Poly(arylene ether)/SiO_2 Composite Membranes with Enhanced Proton Selectivity for Vanadium Redox Flow Batteries

Zhoulin Ye, Nanjie Chen, Zigui Zheng, Lei Xiong * and Dongyang Chen *

School of Materials Science and Engineering, Fuzhou University, Fuzhou 350116, China
* Correspondence: xionglei_fzu@fzu.edu.cn (L.X.); dongyang.chen@fzu.edu.cn (D.C.)

Abstract: Proton exchange membranes (PEMs) are an important type of vanadium redox flow battery (VRFB) separator that play the key role of separating positive and negative electrolytes while transporting protons. In order to lower the vanadium ion permeability and improve the proton selectivity of PEMs for enhancing the Coulombic efficiency of VRFBs, herein, various amounts of nano-sized SiO_2 particles were introduced into a previously optimized sulfonated poly(arylene ether) (SPAE) PEMs through the acid-catalyzed sol-gel reaction of tetraethyl orthosilicate (TEOS). The successful incorporation of SiO_2 was confirmed by FT-IR spectra. The scanning electron microscopy (SEM) images revealed that the SiO_2 particles were well distributed in the SPAE membrane. The ion exchange capacity, water uptake, and swelling ratio of the PEMs were decreased with the increasing amount of SiO_2, while the mechanical properties and thermal stability were improved significantly. The proton conductivity was reduced gradually from 93.4 to 76.9 mS cm^{-1} at room temperature as the loading amount of SiO_2 was increased from 0 to 16 wt.%; however, the VO^{2+} permeability was decreased dramatically after the incorporation of SiO_2 and reached a minimum value of 2.57×10^{-12} m^2 s^{-1} at 12 wt.% of SiO_2. As a result, the H^+/VO^{2+} selectivity achieved a maximum value of 51.82 S min cm^{-3} for the composite PEM containing 12 wt.% of SiO_2. This study demonstrates that the properties of PEMs can be largely tuned by the introduction of SiO_2 with low cost for VRFB applications.

Keywords: proton exchange membrane; sulfonated poly(arylene ether); composite; proton conductivity; vanadium permeability

check for updates

Citation: Ye, Z.; Chen, N.; Zheng, Z.; Xiong, L.; Chen, D. Preparation of Sulfonated Poly(arylene ether)/SiO_2 Composite Membranes with Enhanced Proton Selectivity for Vanadium Redox Flow Batteries. *Molecules* **2023**, *28*, 3130. https://doi.org/10.3390/molecules28073130

Academic Editor: Jean St-Pierre

Received: 16 February 2023
Revised: 25 March 2023
Accepted: 27 March 2023
Published: 31 March 2023

Copyright: © 2023 by the authors. Licensee MDPI, Basel, Switzerland. This article is an open access article distributed under the terms and conditions of the Creative Commons Attribution (CC BY) license (https://creativecommons.org/licenses/by/4.0/).

1. Introduction

Vanadium redox flow batteries (VRFBs), owing to their outstanding merits such as low cost, fast response, high efficiency, good cycling stability, and promising application in large-scale energy storage, have attracted extensive attention over the past decades as the most promising large-scale energy storage units [1–3]. In VRFBs, the proton exchange membrane (PEM) is an important separator between the catholyte and anolyte that prevents the cross-mixing of electrolytes while allowing the migration of conductive ions (H^+ or SO_4^{2-}) to complete the electrical circuit. An ideal PEM should possess high ion conductivity, low vanadium permeability, robust mechanical strength, and good chemical stability [4,5]. Nafion membranes, a typical perfluorinated sulfonic acid membrane developed by DuPont, have been widely acknowledged as the benchmark material for VRFBs due to their high proton conductivity and excellent chemical stability. However, the challenge of achieving high vanadium permeability in Nafion membranes, as well as their low ion selectivity and high cost, still restrict their large-scale application in VRFBs [6–9]. Alternatively, sulfonated fluorinated aromatic polymers, such as sulfonated poly(arylene ether ketone) (SPAEK) [10–12], sulfonated polyimide (SPI) [13–15], and sulfonated polysulfone (SPSF) [16,17], have attracted much attention due to their excellent comprehensive performance, low cost, and easy preparation [18–22].

Organic–inorganic composite PEMs combine the advantages of organic polymers and inorganic fillers [23]. They are usually prepared by incorporating inorganic filling materials such as SiO_2, TiO_2, and graphene oxide (GO) into PEMs. Many research groups have developed this type of composite PEM with excellent performance. For example, Xi et al. [24] prepared Nafion/SiO_2 composite membrane using the sol–gel method, and the doped SiO_2 particles (9.2 wt.%) were distributed in the hydrophilic channel network of Nafion 117. Compared with those of unmodified Nafion 117, slightly reduced water uptake (26.0% vs. 21.5%) and proton conductivity (58.7 mS cm^{-1} vs. 56.2 mS cm^{-1}) were achieved for the composite PEMs with significantly reduced vanadium ion permeability under similar IEC. The VRFB assembled with Nafion/SiO_2 hybrid membranes showed higher Coulombic efficiency and energy efficiency together with a lower self-discharge rate than the VRFB assembled with Nafion 117. Hossain and Aziz et al. [25] prepared SPAEK/$Ce_2Zr_2O_7$ composite membrane by doping $Ce_2Zr_2O_7$ nano-oxide into SPAEK solution. The vanadium ion permeability of the composite membrane was 27 and 12 times lower than those of the pristine Nafion 212 and SPAEK membranes, respectively. These literature studies show that the physicochemical properties of PEMs can be improved by introducing inorganic nanofillers. The inorganic nanoparticles not only have stable chemical properties but also can be easily mixed into the ion transporting channel of PEMs due to their hydrophilicity and small size, which can effectively inhibit the permeation of vanadium ions and improve the proton selectivity of PEMs [26–34].

For the real commercialization of VRFBs, the cost of its separator is critically important. While many high-performance PEMs can be prepared from specially designed polymers and fillers [35–39], the cost associated with the full synthesis process may be very high. In addition, those syntheses may not be easily scaled up. To address these challenges, herein, we adopt an economic way to incorporate SiO_2 into a previously optimized sulfonated poly(arylene ether) (SPAE) PEM [40] via the acid-catalyzed sol-gel reaction of TEOS. SPAE was selected because of its higher Coulombic efficiency and energy efficiency compared to Nafion 212 when assembled in VRFBs, which is realized by its ion-clustered macromolecular structure with distinct phase separation. SiO_2 was selected as a dopant due to its ease of synthesis, low cost, and excellent chemical stability in the electrolytes of VRFBs. The influence of the amount of SiO_2 on the ion exchange capacity, water uptake, swelling ratio, tensile strength, elongation-at-break, proton conductivity, vanadium ion permeability, and thermal stability of the membranes was investigated in detail.

2. Results and Discussion

2.1. Preparation of the SPAE/SiO_2 Composite PEMs

Due to the high surface energy, nano-SiO_2 agglomerates easily, making it difficult to disperse uniformly in a polymer matrix. Herein, various amounts of SiO_2 were introduced into SPAE by acid-catalyzed sol-gel reaction of TEOS, as depicted in Figure 1. After ultrasonic dispersion and mechanical agitation, uniform mixtures were formed, and the SPAE/SiO_2 composite PEMs were successfully cast from these mixtures. The hydrophilic SiO_2 particles were expected to fill in the hydrophilic channels of SPAE, thus increasing the tortuosity of the hydrophilic channels and depressing the permeability of vanadium ions to mitigate the capacity decay and increase the Coulombic efficiency of VRFBs.

The incorporation of SiO_2 into SPAE was confirmed by FT-IR spectra, as shown in Figure 2. The characteristic uptake peaks of SiO_2 appeared at 1087 cm^{-1} (asymmetric stretching of Si-O-Si), 797 and 470 cm^{-1} (symmetric stretching of Si-O), confirming the successful incorporation of SiO_2 into SPAE. It should be noted that the absorption peaks of SPAE are almost unchanged after the incorporation of SiO_2, even though the -OH groups on SiO_2 may form hydrogen bonds with the -SO_3H on SPAE. This may be because the hydrogen bonding within SPAE is much stronger than the hydrogen bonding between SiO_2 and SPAE.

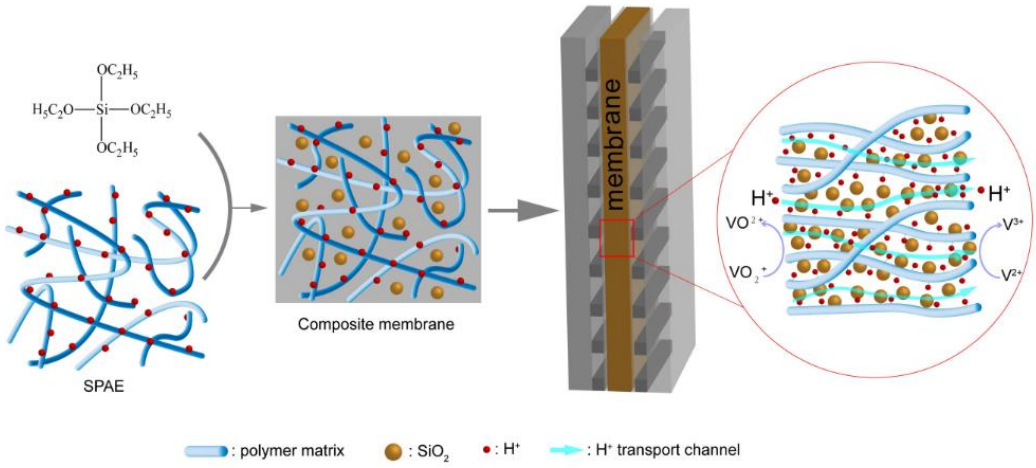


Figure 1. Schematic of VRFB based on the prepared SPAE/SiO_2 composite PEMs.

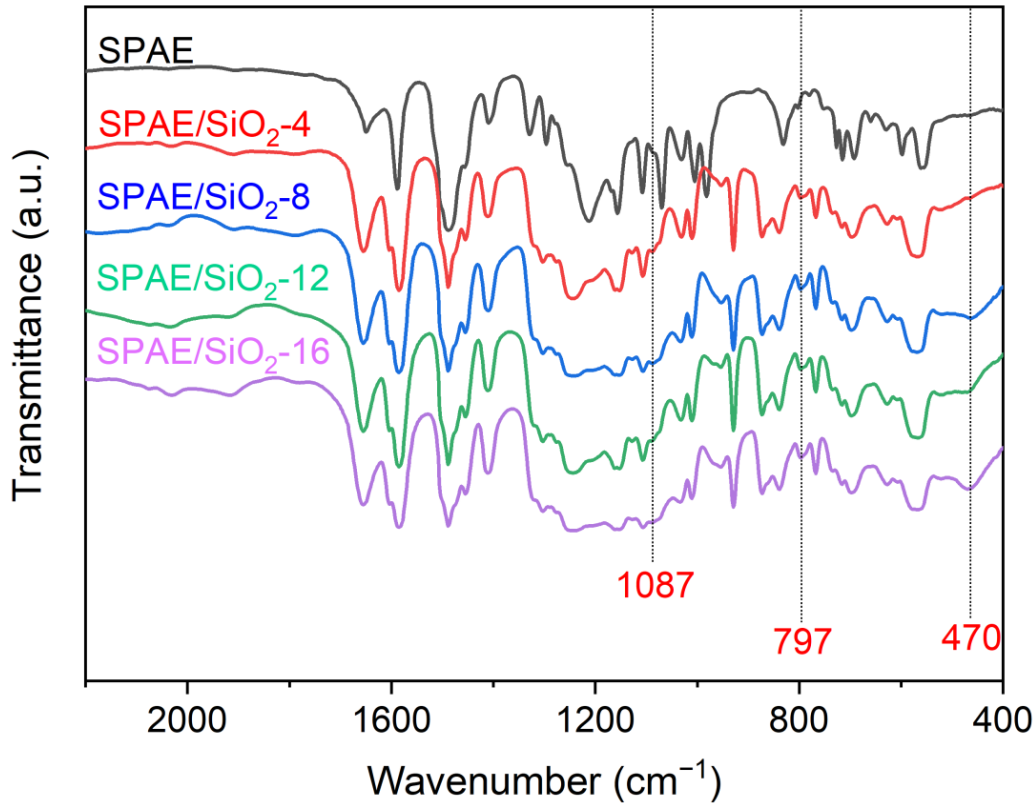


Figure 2. FT-IR spectra of the SPAE and SPAE/SiO_2 composite PEMs.

2.2. Microstructure of the SPAE/SiO_2 Composite PEMs

The upper surface, lower surface, and cross-section morphology of the pristine SPAE and the SPAE/SiO_2 composite PEMs were investigated by SEM, as shown in Figure 3. The surface in contact with air during casting was the upper surface, and the surface in contact with the glass substrate was the lower surface. The SiO_2 particles can be seen in the SEM images of the SPAE/SiO_2 composite PEMs without obvious agglomeration, even though the size of SiO_2 particles increases with the increase of SiO_2 content. Slight sedimentation of SiO_2 particles on the lower surface can be seen, which can be ascribed to gravity during the casting process. The introduction of SiO_2 particles into the polymer matrix does not introduce porosity, indicating good contact between the polymer matrix and filler. These results suggest that the SiO_2 particles are well dispersed in the SPAE/SiO_2 composite PEMs.

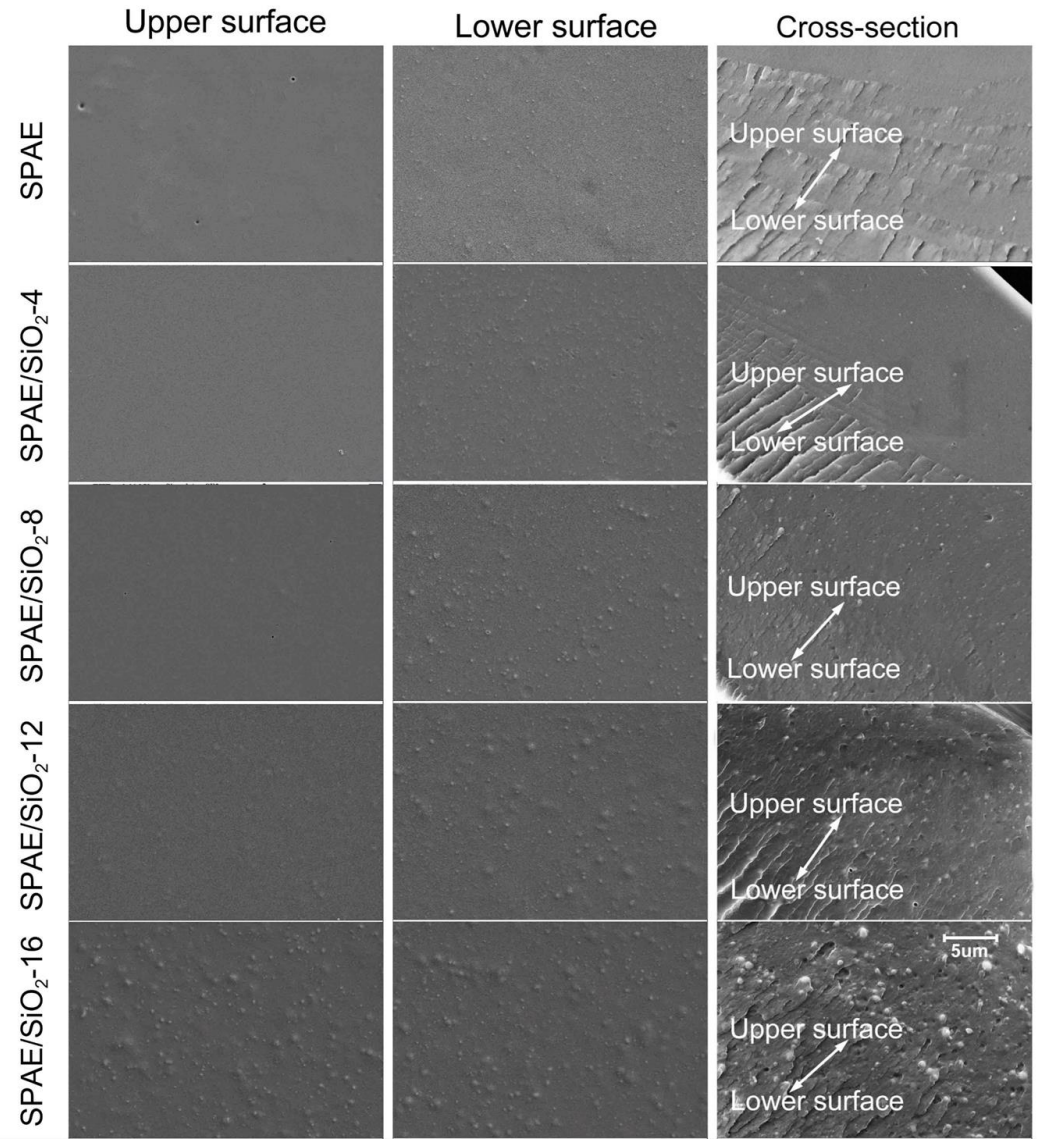


Figure 3. SEM images of the SPAE and SPAE/SiO_2 composite PEMs.

2.3. IEC, Water Uptake, and Swelling Ratio

The IEC, water uptake, and swelling ratio of the prepared membranes at room temperature are listed in Table 1. The IEC of the pristine SPAE is 1.97 mmol g^{-1}, and that of the SPAE/SiO_2 composite PEMs varies in the range of 1.70–1.90 mmol g^{-1} due to the addition of different mass fractions of SiO_2. The water uptake and swelling ratio of the SPAE/SiO_2 composite PEMs decreased gradually with the increase of SiO_2 content, which was because of the lowered IEC after the incorporation of SiO_2. Specifically, the water uptake and swelling ratio of the SPAE were 25.6 and 13.3%, respectively, and decreased to 15.2 and 8.7%, respectively, for the SPAE/SiO_2-16 (IEC = 1.70 mmol g^{-1}).

The water uptake and swelling ratio of pristine SPAE and SPAE/SiO_2 composite PEMs as a function of temperature are plotted in Figure 4. It can be seen that all of the prepared membranes absorb more water at elevated temperatures, leading to higher water uptake (Figure 4a) and swelling ratio (Figure 4b). This is a common physicochemical phenomenon for ionomers as the interaction between water and ionomers is enhanced at high temperatures [41]. If the mass of SiO_2 from the composite membrane is deducted to calculate the actual water uptake of the polymer itself, the actual water uptake of the polymer component in the SPAE/SiO_2-16 is 17.6%, which is also much lower than the pristine SPAE (25.6%). The result implies that doping SiO_2 can significantly inhibit the

water uptake of the membrane. Since there is no chemical bonding between SPAE and SiO_2, the reduced water uptake may be ascribed to the surface confinement of SiO_2, which restricts the polymer chains from being swelled by water molecules.

Table 1. Basic properties of the SPAE and SPAE/SiO_2 composite PEMs at room temperature.

Polymer	IEC (mmol g^{-1})	Water Uptake (%)	Swelling Ratio (%)	Tensile Strength (MPa)	Elongation at Break (%)
SPAE	1.97	25.6	13.3	26.33	24.8
SPAE/SiO_2-4	1.90	23.5	11.6	27.28	21.5
SPAE/SiO_2-8	1.82	21.6	10.5	31.01	18.3
SPAE/SiO_2-12	1.76	18.3	9.6	37.03	15.0
SPAE/SiO_2-16	1.70	15.2	8.7	29.13	9.7

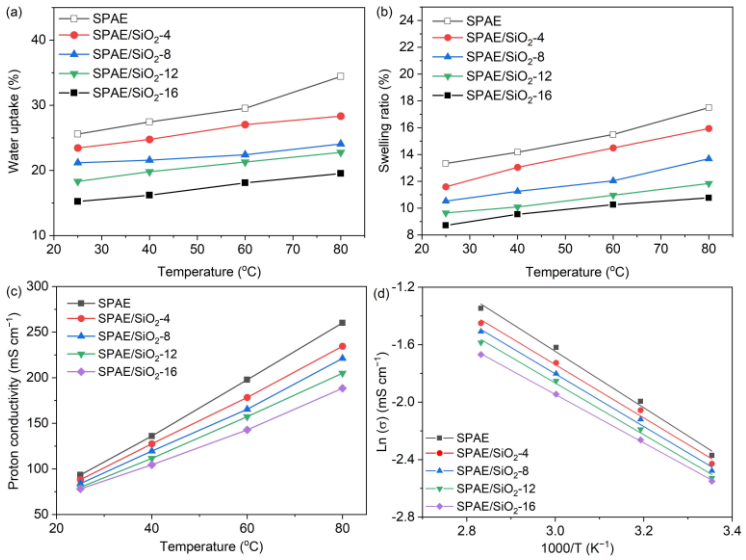


Figure 4. (**a**) Water uptake and (**b**) swelling ratio of the SPAE and SPAE/SiO_2 composite PEMs as a function of temperature, (**c**) proton conductivity, and (**d**) Arrhenius plots of the SPAE and SPAE/SiO_2 composite PEMs.

2.4. Proton Conductivity and Area Resistance

Proton conductivity is a core property of PEMs, which is mainly affected by IEC, ion distribution, and water uptake [42]. The proton conductivity (σ) of the prepared membranes was evaluated in deionized water at various temperatures; the relationship between proton conductivity and temperature is shown in Figure 4c,d. In general, the proton conductivity increases with the increase in temperature owing to the increased free volume of the matrix and the activated proton migration at higher temperatures. The proton conductivity of the SPAE/SiO_2 composite PEMs decreases with the increase of SiO_2 content. At room temperature, the proton conductivity decreases from 93.4 mS cm^{-1} for SPAE to 76.9 mS cm^{-1} for SPAE/SiO_2-16, as listed in Table 2. For comparison, the proton conductivity of Nafion 212 is 85.0 mS cm^{-1} at room temperature, which is slightly lower than that of SPAE. The apparent activation energy (E_a) was calculated from the slope of Arrhenius plots (ln σ vs. 1000/T curves), as shown in Figure 4d [43], and the results are listed in Table 2. The E_a values of the composite PEMs are in the range of 14.03–15.58 kJ mol^{-1}, indicating that the incorporation of SiO_2 into the membrane does not increase the E_a; instead, it lowers the E_a slightly. This implies that the hydrophilic SiO_2 may facilitate the dissociation and hopping of protons. The area resistance of the prepared membranes increases with the increase of SiO_2 content, as listed in Table 2. With the increase of SiO_2 content from 4 wt.% to 16 wt.%, the area resistance of the SPAE/SiO_2

composite PEMs increases from 0.87 Ω cm^2 to 1.59 Ω cm^2, suggesting that the introduction of SiO_2 sacrifices the area resistance.

Table 2. Properties of the SPAE and SPAE/SiO_2 composite PEMs at room temperature.

Polymer	Thickness (μm)	σ (mS cm^{-1})	Ea (KJ mol^{-1})	Area Resistance (Ω cm^2)	VO^{2+} Permeability (10^{-12} m^2 s^{-1})	Ion Selectivity (10^3 S min cm^{-3})
SPAE	58	93.4	16.31	0.71	7.62	20.42
SPAE/SiO_2-4	53	88.2	15.58	0.87	6.11	24.06
SPAE/SiO_2-8	55	83.9	15.44	0.93	4.31	32.44
SPAE/SiO_2-12	51	79.9	15.00	1.17	2.57	51.82
SPAE/SiO_2-16	50	76.9	14.03	1.59	3.64	35.21

2.5. Thermal and Mechanical Properties

The thermal stability of the prepared membranes was investigated by thermogravimetric analysis (TGA) under N_2 atmosphere. Prior to measurements, all samples were held at 150 °C for 30 min. to remove any absorbed water and residual solvents. As shown in Figure 5a, two steps of weight loss can be found for the pristine SPAE and SPAE/SiO_2 composite PEMs. The first step of weight loss (300~360 °C) can be attributed to the decomposition of sulfonic acid groups, while the second step of weight loss (>480 °C) can be attributed to the decomposition of the polymer backbone. The 5% weight-loss temperature ($T_{d\text{-}5\%}$) for SPAE is 345 °C, and the $T_{d\text{-}5\%}$ of the SPAE/SiO_2 composite PEMs increases with the increase of SiO_2 content. Therefore, the introduction of the thermally stable SiO_2 enhances the thermal stability of the PEM.

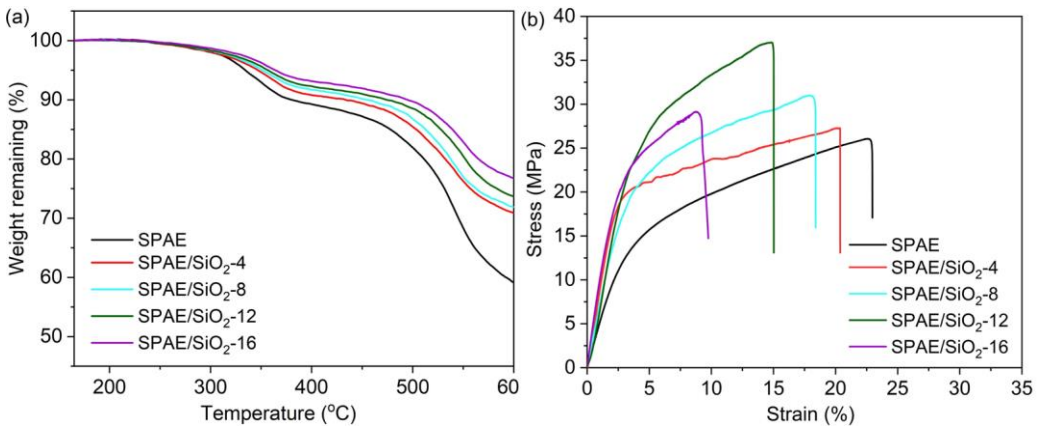


Figure 5. (**a**) TGA curves and (**b**) strain–stress curves of the SPAE and SPAE/SiO_2 composite PEMs.

The mechanical strength of PEMs is critically important for practical applications. The stress-strain curves of the SPAE and SPAE/SiO_2 composite PEMs are shown in Figure 5b, and the corresponding tensile strength and elongation at break are listed in Table 1. The tensile strength of the SPAE/SiO_2 composite PEMs increases as the SiO_2 content is increased from 0 to 12 wt.%, then decreases as the SiO_2 content is further increased to 16 wt.%. The sudden decrease in tensile strength of SPAE/SiO_2-16 may be ascribed to the relative aggregation of nano-sized SiO_2 at this doping amount. The elongation at break of the SPAE/SiO_2 composite PEMs decreases with the increase of SiO_2 content. Therefore, the introduction of SiO_2 generally increases the stiffness of the membrane. Since the SPAE matrix is very flexible, the introduction of a moderate amount of SiO_2 is still advantageous for VRFB applications.

2.6. VO^{2+} Permeability and Ion Selectivity

The vanadium ion permeability of PEMs affects the Coulombic efficiency and capacity decay of the VRFBs [44]. Since both vanadium ions and protons are cations, the vanadium ion permeability of PEMs is usually significant. Doped nanohybrids can fill in the ion transport channels of PEMs and act as barriers to vanadium ions by increasing the tortuosity of the channels; therefore, they have received much attention [45]. Since the Stokes radius of hydrated protons is significantly smaller than the hydrated vanadium ions, the proton conductivity can be much less influenced by the introduction of nanofillers [46]. The permeation of VO^{2+} through the SPAE and SPAE/SiO_2 composite PEMs was recorded, as shown in Figure 6a. Linear permeation of VO^{2+} as a function of time can be found, which follows Fick's law of diffusion. The VO^{2+} permeabilities of the SPAE and SPAE/SiO_2 composite PEMs were calculated, as shown in Table 2 and Figure 6b. The VO^{2+} permeability of SPAE is 7.62×10^{-12} m^2 s^{-1}, which is greater than that of Nafion 212 (5.36×10^{-12} m^2 s^{-1}). The VO^{2+} permeability of the composite PEMs decreases gradually with the introduction of SiO_2 until the SiO_2 content is 12% and then increases slightly when the SiO_2 content is further increased to 16%. SPAE/SiO_2-12 has the lowest VO^{2+} permeability of 2.57×10^{-12} m^2 s^{-1}. For SPAE/SiO_2-16, the VO^{2+} permeability is 3.64×10^{-12} m^2 s^{-1}, which may be ascribed to the relative aggregation of SiO_2 in the membrane, resulting in a lowered blocking capability. Therefore, the introduction of SiO_2 is effective in suppressing the permeation of VO^{2+}, and the best doping content is 12% for the SPAE/SiO_2 composite PEMs. Since the permeations of V^{2+}, V^{3+}, and VO_2^+ are similar to the permeation of VO^{2+}, the VO^{2+} permeability is usually selected as a representative parameter for PEM evaluations [10]. For practical applications, the permeation of all four valence states of vanadium ions, driven not only by the concentration gradient but also by the electric field, should be considered together.

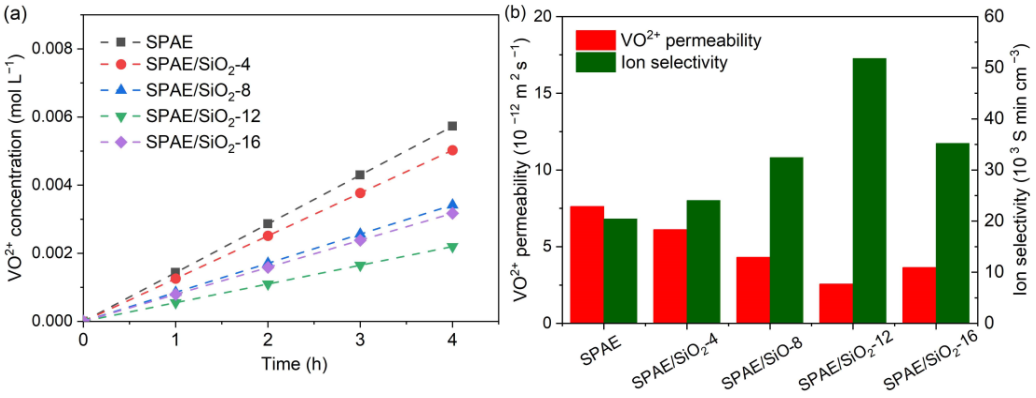


Figure 6. (**a**) Permeated VO^{2+} concentration as a function of time and (**b**) VO^{2+} permeability and ion selectivity of the SPAE and SPAE/SiO_2 composite PEMs.

The ion (H^+/VO^{2+}) selectivities of the SPAE and SPAE/SiO_2 composite PEMs are shown in Table 2 and Figure 6b. While the SPAE/SiO_2 composite PEMs have slightly lower proton conductivity than the pristine SPAE, their VO^{2+} permeability is remarkably lower. Therefore, their ion selectivity is much higher than the pristine SPAE. This can be attributed to the increased tortuosity of the proton conducting channels for the composite PEMs. The ion selectivity of the SPAE/SiO_2 composite PEMs first increases with the increase of SiO_2 content, from 24.06 S min cm^{-3} for SPAE/SiO_2-4 to 51.82 S min cm^{-3} for SPAE/SiO_2-12 at room temperature, and then decreases to 35.21 S min cm^{-3}. The SPAE/SiO_2-12 has the highest ion selectivity (nearly 1.5 times higher than the pristine SPAE) because of its balanced proton conductivity and VO^{2+} permeability. For comparison, the ion selectivity of Nafion 212 is only 15.84 S min cm^{-3}. It has been reported that the incorporation of SiO_2 [47], amino-SiO_2 [48], sulfated ZrO_2 [49], sulfonated graphene oxide [50], and phosphotungstic acid immobilized Kevlar fibers [51] can increase the ion selectivity of PEMs for VRFB applications. The ion selectivity of SPAE/SiO_2-12 is comparable to or even higher than

those of the composite PEMs in the cited literature. Given the ease of preparation and low cost, SPAE/SiO_2-12 is an attractive candidate PEM for the commercialization and long-term operation of VRFBs.

2.7. Oxidative Stability

The oxidative stability of the PEMs can be evaluated ex situ by immersing the samples in the oxidative VRFB catholyte [52]. The color change of the catholyte and the weight change of the samples are two important indications of relative stability. As shown in Figure 7a, the initial color of the VRFB catholyte is yellow. After 15 days of immersions with Nafion 212, SPAE, and SPAE/SiO_2 composite PEMs, the colors of the VRFB catholytes are nearly unchanged. When the immersion time is extended to 60 days, the color of the VRFB catholyte with Nafion 212 is still yellow; however, the colors of the VRFB catholytes with SPAE and SPAE/SiO_2 composite PEMs change to light blue, suggesting that some degradation has taken place. The colors are almost the same for the SPAE and SPAE/SiO_2 composite PEMs, suggesting that their degradation rate is similar. After 60 days of immersion, all the samples remain intact, and the weight loss of the SPAE is 7.4%, while that of the composite PEMs range from 6.4 to 7.0%. The smaller weight loss of the composite PEMs may be attributed to their reduced water uptake, which lowers the amount of the oxidative VO_2^+ species diffusing into the membranes to carry out the degradation inside.

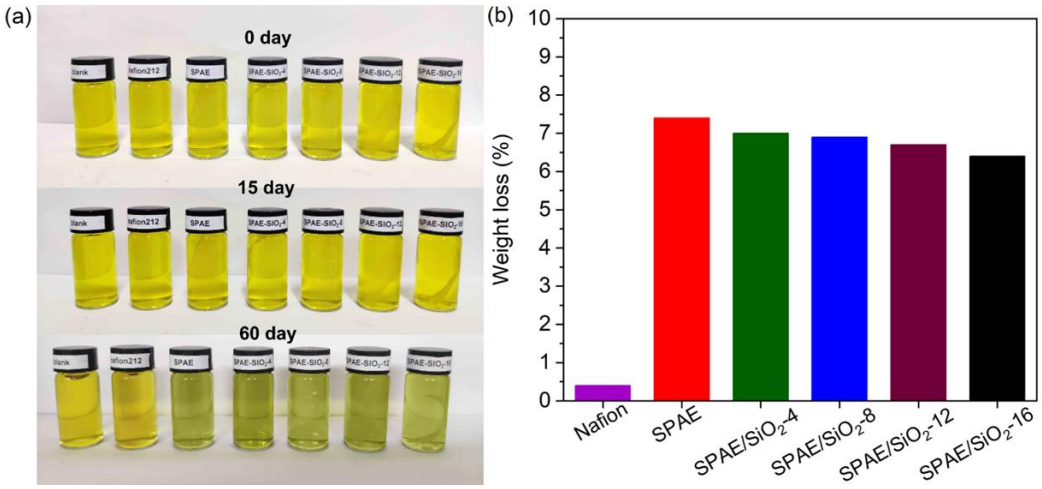


Figure 7. (**a**) Digital photos of Nafion 212, SPAE, and SPAE/SiO_2 composite PEMs in 1.0 M VO^{2+} + 2.0 M H_2SO_4 solution at the 0, 15, and 60 days; (**b**) weight loss of Nafion 212, SPAE, and SPAE/SiO_2 composite PEMs after 30 days of immersion.

3. Experimental Section

3.1. Materials

Sulfonated poly(arylene ether) (SPAE) with an ion exchange capacity (IEC) of 1.97 mmol g^{-1} was synthesized according to our previous report [40]. Other chemicals were obtained from commercial sources and used as received.

3.2. Preparation of SPAE/SiO_2 Composite PEMs

SiO_2 was introduced into SPAE solution by sol-gel reaction of TEOS [53], and the doping degree was controlled by adjusting the added amount of TEOS. The specific steps are as follows. Firstly, SPAE was acidified with 1 M sulfuric acid solution and purified by dissolving in *N*,*N*′-dimethylacetamide (DMAc), filtering to remove insoluble impurities, and drying in an oven. Then, 1.0 g of SPAE was dissolved in 20 mL of DMAc, and a certain amount of TEOS was added dropwise with a liquid transfer gun and ultrasonicated for 0.5 h. The pH of the mixture was adjusted to 4 by adding 0.1 M sulfuric acid solution. The mixture was stirred for 24 h, cast on a horizontal glass plate, dried at 80 °C for 12 h,

then dried at 80 °C under vacuum for another 12 h. Finally, the glass plate was immersed in deionized water, and the membrane was peeled off. The membranes were noted as SPAE/SiO_2−x composite PEMs, where x represents the mass percentage of SiO_2. These composite PEMs were acidified with 1 M sulfuric acid solution and stored in deionized water for further use. All the composite PEMs with different doping levels were prepared with the same polymer mass and the same size of the glass substrate, so the thickness of the membranes showed little difference, all lying in the range of 50–55 μm.

3.3. Characterizations

Fourier transform infrared spectroscopy (FT-IR, Nicolet 5700, Thermo Fisher, MA, USA) was recorded at 4000–400 cm^{-1}, 32 times s^{-1}, resolution 0.2 cm^{-1}. Thermal stabilities were analyzed using a thermogravimetric analyzer (TGA, SDT-Q600, TA Instruments, New Castle, DE, USA) with a heating rate of 10 °C min^{-1} under a nitrogen atmosphere (flow rate: 20 mL min^{-1}), and the samples were conditioned at 150 °C for 30 min. to remove the residual solvent and water. The morphologies of the membranes were investigated by scanning electron microscopy (SEM, SUPRA 55, Zeiss, Jena, Germany). The samples were sprayed with gold to increase conductivity.

3.3.1. Water Uptake and Swelling Ratio

Water uptake and swelling ratio of membranes were measured at 25, 40, 60, and 80 °C. The samples were immersed in deionized water and equilibrated at the corresponding testing temperature for 24 h. The water uptake and swelling ratio were then calculated from the following equations:

$$Water\ uptake(\%) = \frac{W_{wet} - W_{dry}}{W_{dry}} \times 100 \quad (1)$$

$$Swelling\ ratio(\%) = \frac{L_{wet} - L_{dry}}{L_{dry}} \times 100 \quad (2)$$

where W_{wet} and W_{dry} are the wet and dry mass of the samples, respectively; L_{wet} and L_{dry} are the wet and dry lengths of the samples, respectively.

3.3.2. Oxidative Stability

Oxidative stability was evaluated under acidic conditions by immersing the membranes in 1.0 M VO^{2+} + 2.0 M H_2SO_4 solution at room temperature for 60 days and then recording the weight loss of the sample and the color change of the solution [54].

3.3.3. Mechanical Properties

Mechanical properties were measured by a universal stretching machine (UTM 6502X, SUNS universal testing instrument, Shenzhen, China). Rectangular samples were taken out from deionized water and measured immediately with a stretching rate of 5 mm min^{-1}.

3.3.4. Ion Exchange Capacity (IEC)

The IEC values of composite membranes were measured by acid-base titration. The composite membrane was immersed in 1 M of Na_2SO_4 solution for 24 h, followed by titration with 0.1 M NaOH solution using phenolphthalein as the indicator. The volume of consumed NaOH solution was recorded. The formula was as follows.

$$IEC = \frac{\Delta V_{NaOH} \times C_{NaOH}}{W_{dry}} \quad (3)$$

where ΔV_{NaOH} is the consumed volume of NaOH solution, C_{NaOH} is the concentration of NaOH solution, and W_{dry} is the weight of the dry sample.

3.3.5. Proton Conductivity

The proton conductivities were measured by AC impedance spectroscopy using an impedance/gain phase analyzer (Solartron 1260, Ametek, Newark, DE, USA) in a frequency range from 1 to 10 MHz [55,56]. The conductivities were calculated as follows [57,58].

$$\sigma = \frac{L}{RS} \tag{4}$$

where L is the distance between two electrodes, R is the resistance of hybrid membranes, and S is the transverse area of the composite membranes.

3.3.6. Area Resistance

The area resistances were measured according to the method reported in the literature [59]. Before testing, the composite membranes were soaked in 1.0 M VO^{2+} + 2.0 M H_2SO_4 solution for 24 h. When starting to test, the membrane was clamped between two compartments filled with the 1.0 M VO^{2+} + 2.0 M H_2SO_4 solution. The effective measuring area of the membrane (S) was 2.41 cm^2. When testing the resistance of the device with membrane (R_1) and without membrane (R_2), respectively, the area resistances (AR) were calculated as follows.

$$AR = (R_1 - R_2) \times S \tag{5}$$

3.3.7. VO^{2+} Permeability and Ion Selectivity

The VO^{2+} permeabilities were measured according to the method reported in the literature [60]. The membrane was clamped between a two-compartment diffusion cell (containing 80 mL of 1.0 M $VOSO_4$ + 2.0 M H_2SO_4 solution and 80 mL of 1.0 M $MgSO_4$ + 2.0 M H_2SO_4 solution). A volume of 1 mL of solution from the $MgSO_4$ cell was taken out every 1 h at room temperature and titrated using an ultraviolet spectrophotometer (UV−5800 HPC, METASH, Shanghai, China, wavelength: 765 nm) to give the concentration of VO^{2+}. The VO^{2+} permeabilities were calculated using the Formula (6) [61,62].

$$V_B \frac{dC_B(t)}{dt} = A\frac{D}{L}(C_A - C_B(t)) \tag{6}$$

where A (cm^2) and L (cm) are effective membrane area and the membrane thickness, t (s) is testing time, D is the VO^{2+} permeabilities, C_A and C_B (mol/L) are initial concentration of VO^{2+} in $VOSO_4$ and $MgSO_4$ solution, respectively, and V_B (mL) is the volume of $MgSO_4$. The ion selectivity was defined as the ratio of proton conductivity over VO^{2+} permeability.

4. Conclusions

Various amounts of nano-sized SiO_2 particles were successfully introduced into a previously optimized sulfonated poly(arylene ether) (SPAE) PEM through the acid-catalyzed sol-gel reaction of tetraethyl orthosilicate (TEOS). FT-IR spectra and SEM images confirmed the presence of SiO_2 in the SPAE matrix. With the increase in SiO_2 amount, the IEC, and water uptake, the swelling ratio of the PEMs decreased, as expected. The proton conductivity reduced gradually from 93.4 to 76.9 mS cm^{-1} at room temperature as the loading amount of SiO_2 was increased from 0 to 16 wt.%; however, the VO^{2+} permeability decreased dramatically after the incorporation of SiO_2 and reached a minimum value of 2.57×10^{-12} m^2 s^{-1} at 12 wt.% of SiO_2. As a result, the H^+/VO^{2+} selectivity achieved a maximum value of 51.82 S min cm^{-3} for the SPAE/SiO_2-12. Moreover, the tensile strength and $T_{d\text{-}5\%}$ of SPAE/SiO_2-12 were 37.03 MPa and 359.8 °C, respectively, which were much higher than those of pure SPAE (26.33 MPa and 344.8 °C). Therefore, the optimization of SiO_2 amount is important for composite PEMs to balance the trade-off between proton conductivity and vanadium ion permeability, and SPAE/SiO_2-12 is a promising candidate membrane for VRFB applications.

Author Contributions: Conceptualization, Z.Y. and Z.Z.; methodology, N.C.; investigation, Z.Y. and Z.Z.; writing—original draft preparation, Z.Y. and L.X.; writing—review and editing, D.C.; supervision, D.C.; funding acquisition, D.C. All authors have read and agreed to the published version of the manuscript.

Funding: This study was supported by the National Natural Science Foundation of China (51873037) and the Natural Science Foundation of Fujian Province (2020J01475).

Data Availability Statement: The data presented in this study are available on request from the corresponding author.

Conflicts of Interest: The authors declare no conflict of interest.

Sample Availability: Samples of all compounds are available from the authors.

References

1. Choi, C.; Kim, S.; Kim, R.; Choi, Y.; Jung, H.Y.; Yang, J.H.; Kim, H.T. A review of vanadium electrolytes for vanadium redox flow batteries. *Renew. Sust. Energ. Rev.* **2017**, *69*, 263–274. [CrossRef]
2. Schwenzer, B.; Zhang, J.L.; Kim, S.; Li, L.Y.; Liu, J.; Yang, Z.G. Membrane development for vanadium redox flow batteries. *ChemSusChem* **2011**, *4*, 1388–1406. [CrossRef] [PubMed]
3. Chen, D.Y.; Hickner, M.A.; Agar, E.; Kumbur, E.C. Selective anion exchange membranes for high coulombic efficiency vanadium redox flow batteries. *Electrochem. Commun.* **2013**, *26*, 37–40. [CrossRef]
4. Zhang, S.H.; Yin, C.X.; Xing, D.B.; Yang, D.L.; Jian, X.G. Preparation of chloromethylated/quaternized poly(phthalazinone ether ketone) anion exchange membrane materials for vanadium redox flow battery applications. *J. Membr. Sci.* **2017**, *363*, 243–249. [CrossRef]
5. Xi, J.Y.; Jiang, B.; Yu, L.H.; Liu, L. Membrane evaluation for vanadium flow batteries in a temperature range of −20–50 °C. *J. Membr. Sci.* **2017**, *522*, 45–55. [CrossRef]
6. Wu, C.X.; Lu, S.F.; Wang, H.N.; Xu, X.; Peng, S.K.; Tan, Q.L.; Xiang, Y. A novel polysulfone-polyvinylpyrrolidone membrane with superior proton-to-vanadium ion selectivity for vanadium redox flow batteries. *J. Mater. Chem. A* **2016**, *4*, 1174–1179. [CrossRef]
7. Amel, A.; Smedley, S.B.; Dekel, D.R.; Hickner, M.A.; Ein-Eli, Y. Characterization and chemical stability of anion exchange membranes cross-linked with polar electron-donating linkers. *J. Electrochem. Soc.* **2015**, *162*, 1047–1055. [CrossRef]
8. Sata, T. Studies on anion exchange membranes having permselectivity for specific anions in electrodialysis-effect of hydrophilicity of anion exchange membranes on perm selectivity of anions. *J. Membr. Sci.* **2000**, *167*, 1–31. [CrossRef]
9. Monopoli, A.; Casiello, M.; Cotugno, P.; Milella, A.; Palumbo, F.; Fracassi, F.; Nacci, A. Synthesis of tailored perfluoro unsaturated monomers for potential applications in proton exchange membrane preparation. *Molecules* **2021**, *26*, 5592. [CrossRef]
10. Yang, S.; Ahn, Y.; Kim, D. Poly(arylene ether ketone) proton exchange membranes grafted with long aliphatic pendant sulfonated groups for vanadium redox flow batteries. *J. Mater. Chem. A* **2017**, *5*, 2261–2270. [CrossRef]
11. Cheng, H.L.; Xu, J.M.; Ma, L.; Xu, L.S.; Liu, B.J.; Wang, Z.; Zhang, H.X. Preparation and characterization of sulfonated poly(arylene ether ketone) copolymers with pendant sulfoalkyl groups as proton exchange membranes. *J. Power Sources* **2014**, *260*, 307–316. [CrossRef]
12. Zhang, W.M.; Chen, S.Y.; Chen, D.Y.; Ye, Z.L. Sulfonated binaphthyl-containing poly(arylene ether ketone)s with rigid backbone and excellent film-forming capability for proton exchange membranes. *Polymers* **2019**, *10*, 1287. [CrossRef] [PubMed]
13. Suryani; Chang, Y.N.; Lai, J.Y.; Liu, Y.L. Polybenzimidazole(PBI)-functionalized silica nanoparticles modified PBI nanocomposite membranes for proton exchange membranes fuel cells. *J. Membr. Sci.* **2012**, *403*, 1–7. [CrossRef]
14. Lee, K.H.; Lee, S.Y.; Shin, D.W.; Wang, C.Y.; Ahn, S.H.; Lee, K.J.; Guiver, M.D.; Lee, Y.M. Structural influence of hydrophobic diamine in sulfonated poly(sulfide sulfone imide) copolymers on medium temperature PEM fuel cell. *Polymer* **2014**, *55*, 1317–1326. [CrossRef]
15. Duburg, J.C.; Azizi, K.; Primdahl, S.; Hjuler, H.A.; Zanzola, E.; Schmidt, T.J.; Gubler, L. Composite polybenzimidazole membrane with high capacity retention for vanadium redox flow batteries. *Molecules* **2021**, *26*, 1679. [CrossRef]
16. Bae, B.; Miyatake, K.; Watanabe, M. Effect of the hydrophobic component on the properties of sulfonated poly(arylene ether sulfone)s. *Macromolecules* **2009**, *42*, 1873–1880. [CrossRef]
17. Kim, Y.S.; Hickner, M.A.; Dong, L.M.; Pivovar, B.S.; McGrath, J.E. Sulfonated poly(arylene ether sulfone) copolymer proton exchange membranes: Composition and morphology effects on the methanol permeability. *J. Membr. Sci.* **2004**, *243*, 317–326. [CrossRef]
18. Semiz, L.; Sankir, N.; Sankir, M. Directly copolymerized disulfonated poly(arylene ether sulfone) membranes for vanadium redox flow batteries. *Int. J. Electrochem. Sci.* **2014**, *9*, 3060–3067.
19. Wang, C.; Shin, D.W.; Lee, S.Y.; Kang, N.R.; Lee, Y.M.; Guiver, M.D. Poly(arylene ether sulfone) proton exchange membranes with flexible acid side chains. *J. Membr. Sci.* **2012**, *421*, 375. [CrossRef]
20. Park, C.H.; Lee, C.H.; Guiver, M.D.; Lee, Y.M. Sulfonated hydrocarbon membranes for medium-temperature and low-humidity proton exchange membrane fuel cells (PEMFCs). *Prog. Polym. Sci.* **2011**, *36*, 1443–1498. [CrossRef]

21. Miyatake, K.; Chikashige, Y.; Higuchi, E.; Watanabe, M. Tuned polymer electrolyte membranes based on aromatic poly ethers for fuel cell applications. *J. Am. Chem. Soc.* **2007**, *129*, 3879–3887. [CrossRef] [PubMed]
22. Lee, Y. Fuel cells: Operating flexibly. *Nat. Energy* **2016**, *1*, 16136. [CrossRef]
23. Yang, X.B.; Zhao, L.; Goh, K.; Sui, X.L.; Meng, L.H.; Wang, Z.B. A highly proton-vanadium-selective perfluoro sulfonic acid membrane for vanadium redox flow batteries. *New J. Chem.* **2019**, *43*, 11374–11381. [CrossRef]
24. Xi, J.Y.; Wu, Z.H.; Qiu, X.P.; Chen, L.Q. Nafion/SiO_2 hybrid membrane for vanadium redox flow battery. *J. Power Sources* **2007**, *166*, 531–536. [CrossRef]
25. Hossain, S.I.; Aziz, M.A.; Han, D.B.; Selvam, P.; Shanmugam, S. Fabrication of SPAEK-cerium zirconium oxide nanotube composite membrane with outstanding performance and durability for vanadium redox flow batteries. *J. Mater. Chem. A.* **2018**, *6*, 20205–20213. [CrossRef]
26. Zhang, H.Q.; Yan, X.M.; Gao, L.; Hu, L.; Ruan, X.H.; Zheng, W.J.; He, G.H. Novel triple tertiary amine polymer-based hydrogen bond network inducing highly efficient proton conducting channels of amphoteric membrane for high-performance vanadium redox flow battery. *ACS Appl. Mater. Interfaces* **2019**, *11*, 5003–5014. [CrossRef]
27. Zhang, Y.X.; Wang, H.X.; Qian, P.H.; Zhou, Y.; Shi, J.Y.; Shi, H.F. Sulfonated poly(ether ether ketone)/amine-functionalized graphene oxide hybrid membrane with various chain lengths for vanadium redox flow battery: A comparative study. *J. Membr. Sci.* **2020**, *610*, 118232. [CrossRef]
28. Liu, B.; Jiang, Y.H.; Wang, H.X.; Ge, J.; Shi, H.F. Sulfonated poly(ether ether ketone) hybrid membranes with amphoteric graphene oxide nanosheets as interfacial reinforcement for vanadium redox flow battery. *Energy Fuels* **2020**, *34*, 2452–2461. [CrossRef]
29. Zhang, Y.X.; Wang, H.X.; Liu, B.; Shi, J.L.; Zhang, J.; Shi, H.F. An ultra-high ion selective hybrid proton exchange membrane incorporated with zwitterion-decorated graphene oxide for vanadium redox flow batteries. *J. Mater. Chem. A* **2019**, *7*, 12669–12680. [CrossRef]
30. Zheng, L.Y.; Wang, H.X.; Niu, R.T.; Zhang, Y.X.; Shi, H.F. Sulfonated poly(ether ether ketone)/sulfonated graphene oxide hybrid membrane for vanadium redox flow battery. *Electrochim. Acta* **2018**, *282*, 437–447. [CrossRef]
31. Zhang, Y.X.; Wang, H.X.; Yu, W.K.; Shi, J.L.; Shi, H.F. Sulfonated poly(ether ether ketone)-based hybrid membranes containing polydopamine-decorated multiwalled carbon nanotubes with acid-base pairs for all vanadium redox flow battery. *J. Membr. Sci.* **2018**, *564*, 916–925. [CrossRef]
32. Zhang, Y.X.; Wang, H.X.; Yu, W.K.; Shi, H.F. Structure and properties of sulfonated poly(ether ether ketone) hybrid membrane with polyaniline-chains-modified graphene oxide and its application for vanadium redox flow battery. *ChemistrySelect* **2018**, *3*, 9249–9258. [CrossRef]
33. Niu, R.T.; Kong, L.Q.; Zheng, L.Y.; Wang, H.X.; Shi, H.F. Novel graphitic carbon nitride nanosheets/sulfonated poly(ether ether ketone) acid-base hybrid membrane for vanadium redox flow battery. *J. Membr. Sci.* **2017**, *525*, 220–228. [CrossRef]
34. Kong, L.Q.; Zheng, L.Y.; Niu, R.T.; Wang, H.X.; Shi, H.F. A sulfonated poly(ether ether ketone)/amine-functionalized graphene oxide hybrid membrane for vanadium redox flow batteries. *RSC Adv.* **2016**, *6*, 100262–100270. [CrossRef]
35. Xiong, K.N.; Wu, W.; Wang, S.F.; Zhang, L. Modeling, design, materials and fabrication of bipolar plates for proton exchange membrane fuel cell: A review. *Appl. Energy* **2021**, *301*, 117443. [CrossRef]
36. Elwan, H.A.; Thimmappa, R.; Mamlouk, M.; Scott, K. Applications of poly ionic liquids in proton exchange membrane fuel cells: A review. *J. Power Sources* **2021**, *510*, 230371. [CrossRef]
37. Liu, L.; Wang, C.; He, Z.F.; Das, R.A.J.; Dong, B.B.; Xie, X.F.; Guo, Z.H. An overview of amphoteric ion exchange membranes for vanadium redox flow batteries. *J. Mater. Sci. Technol.* **2021**, *69*, 212–227. [CrossRef]
38. Jing, X.; Li, X.; Han, W. Research progress of proton exchange membranes and electrode materials for all-vanadium flow batteries. *Polym. Bull.* **2021**, *5*, 1–13.
39. Gubler, L. Membranes and separators for redox flow batteries. *Curr. Opin. Electrochem.* **2019**, *18*, 31–36. [CrossRef]
40. Zhang, X.; Li, Z.W.; Chen, X.L.; Chen, D.Y.; Zheng, Y.Y. Side chain engineering of sulfonated poly(arylene ether)s for proton exchange membranes. *Chin. J. Polym. Sci.* **2020**, *38*, 644–652. [CrossRef]
41. Chen, Y.; Li, Y.Y.; Xu, J.Q.; Chen, S.Y.; Chen, D.Y. Densely quaternized fluorinated poly(fluorenyl ether)s with excellent conductivity and stability for vanadium redox flow batteries. *ACS Appl. Mater. Interfaces* **2021**, *13*, 18923–18933. [CrossRef] [PubMed]
42. Yan, J.; Hickner, M. Anion exchange membranes by bromination of benzyl methyl-containing poly(sulfone)s. *Macromolecules* **2010**, *43*, 2349–2356. [CrossRef]
43. Lee, K.H.; Chu, J.Y.; Kim, A.R.; Kim, H.G.; Yoo, D.J. Functionalized TiO2 mediated organic-inorganic composite membranes based on quaternized poly(arylene ether ketone) with enhanced ionic conductivity and alkaline stability for alkaline fuel cells. *J. Membr. Sci.* **2021**, *634*, 119435. [CrossRef]
44. Wiedemann, E.; Heintz, A.; Lichtenthaler, R. Transport properties of vanadium ions in cation exchange membranes: Determination of diffusion coefficients using a dialysis cell. *J. Membr. Sci.* **1998**, *141*, 215–221. [CrossRef]
45. Yang, X.B.; Zhao, L.; Goh, K.; Sui, X.L.; Meng, L.H.; Wang, Z.B. A phosphotungstic acid coupled silica-Nafion composite membrane with significantly enhanced ion selectivity for vanadium redox flow battery. *J. Energy Chem.* **2020**, *41*, 177–184. [CrossRef]
46. Xi, X.L.; Ding, C.; Zhang, H.Z.; Li, X.F.; Cheng, Y.H.; Zhang, H.M. Solvent responsive silica composite nanofiltration membrane with controlled pores and improved ion selectivity for vanadium flow battery application. *J. Power Sources* **2015**, *274*, 1126–1134. [CrossRef]

47. Chen, D.Y.; Wang, S.J.; Xiao, M.; Han, D.M.; Meng, Y.Z. Sulfonated poly (fluorenyl ether ketone) membrane with embedded silica rich layer and enhanced proton selectivity for vanadium redox flow battery. *J. Power Sources* **2010**, *195*, 7701–7708. [CrossRef]
48. Kondratenko, M.S.; Karpushkin, E.A.; Gvozdik, N.A.; Gallyamov, M.O.; Stevenson, K.J.; Sergeyev, V.G. Influence of aminosilane precursor concentration on physicochemical properties of composite Nafion membranes for vanadium redox flow battery applications. *J. Power Sources* **2017**, *340*, 32–39. [CrossRef]
49. Zhang, Y.; Zhou, X.J.; Xue, R.; Yu, Q.C.; Jiang, F.J.; Zhong, Y.G. Proton exchange membranes with ultra-low vanadium ions permeability improved by sulfated zirconia for all vanadium redox flow battery. Int. *J. Hydrog. Energy* **2019**, *44*, 5997–6006. [CrossRef]
50. Rajput, A.; Sharma, P.P.; Yadav, V.; Kulshrestha, V. Highly stable graphene oxide composite proton exchange membrane for electro-chemical energy application. *Int. J. Hydrog. Energy* **2020**, *45*, 16976–16983. [CrossRef]
51. Yang, X.B.; Zhao, L.; Sui, X.L.; Meng, L.H.; Wang, Z.B. Phosphotungstic acid immobilized nanofibers-Nafion composite membrane with low vanadium permeability and high selectivity for vanadium redox flow battery. *J. Colloid Interface Sci.* **2019**, *542*, 177–186. [CrossRef] [PubMed]
52. Chen, D.Y.; Hickner, M.A. V^{5+} degradation of sulfonated Radel membrane for vanadium redox flow batteries. *Phys. Chem. Chem. Phys.* **2013**, *15*, 11299–11305. [CrossRef] [PubMed]
53. Jiang, M.J.; Song, X.Q.; Ye, G.D.; Xu, J.J. Preparation of PVA/paraffin thermal regulating fiber by in situ microencapsulation. *Compos. Sci. Technol.* **2008**, *68*, 2231–2237. [CrossRef]
54. Chen, Y.; Li, Y.Y.; Wang, B.S.; Lin, M.J.; Xie, Z.L.; Chen, D.Y. Fluorinated poly(fluorenyl ether)s with linear multicationic side chains for vanadium redox flow batteries. *Sci. China Mater.* **2021**, *64*, 349–361. [CrossRef]
55. Fujimoto, C.H.; Hickner, M.A.; Cornelius, C.J.; Loy, D.A. Ionomeric poly(phenylene) prepared by Diels-Alder polymerization: Synthesis and physical properties of a novel polyelectrolyte. *Macromolecules* **2005**, *38*, 5010–5016. [CrossRef]
56. Largier, T.; Cornelius, C. Random quaternary ammonium Diels-Alder poly(phenylene) copolymers for improved vanadium redox flow batteries. *J. Power Sources* **2017**, *352*, 149–155. [CrossRef]
57. Ling, X.; Jia, C.K.; Liu, J.G.; Yan, C.W. Preparation and characterization of sulfonated poly (ether sulfone)/sulfonated poly(ether ether ketone) blend membrane for vanadium redox flow battery. *J. Membr. Sci.* **2012**, *415*, 306–312. [CrossRef]
58. Hwang, C.W.; Park, H.M.; Oh, C.M.; Hwang, T.S.; Shim, J.; Jin, C.S. Synthesis and characterization of vinylimidazole-co-trifluoroethylmethacrylate-co-divinylbenzene anion-exchange membrane for all-vanadium redox flow battery. *J. Membr. Sci.* **2014**, *468*, 98–106. [CrossRef]
59. Pang, B.; Zhang, Q.; Xiao, X. Superior acidic sulfate ester group based high conductive membrane for vanadium redox flow battery. *J. Power Sources* **2021**, *506*, 230203. [CrossRef]
60. Shang, X.Y.; Shu, D.; Wang, S.J.; Xiao, M.; Meng, Y.Z. Fluorene-containing sulfonated poly(arylene ether 1,3,4-oxadiazole) as proton-exchange membrane for PEM fuel cell application. *J. Membr. Sci.* **2007**, *291*, 140–147. [CrossRef]
61. Semiz, L.; Demirci, N.; Sankir, M. Influence of the basic membrane properties of the disulfonated poly(arylene ether sulfone) copolymer membranes on the vanadium redox flow battery performance. *J. Membr. Sci.* **2014**, *468*, 209–215. [CrossRef]
62. Liu, S.; Wang, L.H.; Li, D.; Liu, B.Q.; Wang, J.J.; Song, Y.L. Novel amphoteric ion exchange membranes by blending sulfonated poly(ether ether ketone)/quaternized poly(ether imide) for vanadium redox flow battery applications. *J. Mater. Chem. A.* **2015**, *3*, 17590–17597. [CrossRef]

Disclaimer/Publisher's Note: The statements, opinions and data contained in all publications are solely those of the individual author(s) and contributor(s) and not of MDPI and/or the editor(s). MDPI and/or the editor(s) disclaim responsibility for any injury to people or property resulting from any ideas, methods, instructions or products referred to in the content.